Journal of King Saud University – Computer and Information Sciences (2018) 30, 449–461

King Saud University

Journal of King Saud University – Computer and Information Sciences

www.ksu.edu.sa
www.sciencedirect.com

Self-adaptive dragonfly based optimal thresholding for multilevel segmentation of digital images

Rakoth Kandan Sambandam, Sasikala Jayaraman *

Department of Computer Science and Engineering, Annamalai University, Tamil Nadu, India

Received 12 July 2016; revised 27 October 2016; accepted 1 November 2016
Available online 10 November 2016

KEYWORDS

Meta-heuristic algorithms;
Dragonfly optimization;
Multilevel segmentation

Abstract Dragonfly optimization (DFO) is a population based meta-heuristic optimization algorithm that simulates the static and dynamic swarming behaviors of dragonflies. The static swarm comprising less number of dragonflies in a small area for hunting preys, while the dynamic swarm with a large number of dragonflies migrates over long distances; and they represent the exploration and exploitation phases of the DFO. This paper introduces a self adaptive scheme for tuning the DFO parameters and suggests a methodology involving self-adaptive DFO (SADFO) for performing multilevel segmentation of digital images. The multilevel segmentation problem is formulated as an optimization problem and solved using the SADFO. The method optimizes the threshold values through effectively exploring the solution space in obtaining the global best solution. The results of real life and medical images illustrate the performance of the suggested method.

1. Introduction

Image segmentation, a task of dividing an image into several non-overlapping meaningful regions with homogeneous characteristics in respect of texture, gray value, position, etc, has been one of the most difficult and challenging tasks and extensively investigated since 1960s. In other words, it is a process of assigning a label to each pixel in an image, where the pixels with the same label share certain visual characteristics. The segmented regions provide more information than individual pixels since the interpretation of images based on objects is more meaningful than the interpretation based on individual pixels. Image segmentation is considered as an important task in the analysis, interpretation and understanding of images, and widely applied for classification and object recognition in many applications such as fault diagnosis, tracking, monitoring, crack detection, etc. (Skarbek and Koschan, 1994).

In recent years, image segmentation plays a vital role in numerous medical imaging applications such as quantification of tissue volumes, diagnosis, localization of pathology, study of anatomical structure, treatment planning, partial volume correction of functional imaging data and computer integrated surgery. The segmentation methods vary widely depending on the specific application, imaging modality and other factors. For example, the segmentation of brain tissue has different requirements from liver image segmentation. There is thus no single segmentation method that provides acceptable results for all kinds of medical images, thereby making the selection of

* Corresponding author.
E-mail address: sasikala_07@rediffmail.com (S. Jayaraman).
Peer review under responsibility of King Saud University.

Production and hosting by Elsevier

http://dx.doi.org/10.1016/j.jksuci.2016.11.002

an appropriate segmentation method a dilemma. But the radiologists demand a generalized segmentation tool for delineation of anatomical structures and other regions of interest in medical images (Tarabalka et al., 2010; Fauvel et al., 2013).

Numerous segmentation methods have been suggested in the recent decades. These methods can be classified into three categories; threshold-based, deformation-based and clustering-based. The threshold-based methods determine the threshold values using the image histogram and then classify the image pixels based on these values (Otsu, 1979; Kapur et al., 1985; Bonnet et al., 2002; Baradez et al., 2004; Natarajan et al., 2012). Deformation-based methods, employing region growing (Shih and Cheng, 2005; Hojjatoleslami and Kittler, 1998) and level set (Xie et al., 2005; Li et al., 2011) approaches, have been proposed for identification of the cancer boundary. Most of the deformation-based segmentation methods are semiautomatic since the generation of initial points is difficult to automate. The region growing methods group the pixels into homogeneous regions and segment the image into some major areas, while the level set methods utilize dynamic variational boundaries for segmentation; The clustering-based methods segment the feature space of image into several clusters and derive a sketch of the original image, such as K-means (Papamichail and Papamichail, 2007; Clausi, 2002; Juang and Wu, 2010), Fuzzy C-means (FCM) (Carvalho, 2007; Chen and Zhang, 2004; Chuang et al., 2006; Chaira, 2011) and mean-shift (Comaniciu and Meer, 2002) algorithms.

Among the available techniques, thresholding is a simple and effective tool for image segmentation and popular due to lower storage requirement and fast computations. The number of threshold values used for segmentation varies depending on the nature of the application and the type of image. The best threshold number and values are chosen by a trial and error approach. The segmented result should be appropriate, otherwise it may affect the subsequent processes such as feature extraction and classification. The thresholding methods can be partitioned into bi-level and multilevel thresholding depending on the number of thresholds required to be detected (Sezgin and Sankur, 2004). Bi-level thresholding involves one threshold value and creates two classes: one below the threshold and the other above the threshold, while the multi-level thresholding creates nc classes with $nc-1$ threshold levels. These methods employ parametric approach involving gray distribution of the pixels or nonparametric approach requiring an objective function for optimizing the threshold levels. It has been reported (Sezgin and Sankur, 2004) that Kapur's entropy based thresholding offers better performance than any other thresholding approaches.

Nature inspired optimization techniques have been applied for image segmentation in recent years. A dynamic clustering approach based on particle swarm optimization (PSO) that determines optimum number of centroids for image segmentation has been suggested (Omran et al., 2005). A fast image segmentation method based on artificial bee colony (ABC) optimization to estimate the appropriate threshold values in a continuous gray scale interval has been outlined (Ma et al., 2011). A hybrid approach using matched filter and ant colony optimization for extraction of blood vessels in ophthalmoscope images has been presented (Cinsdikici and Aydın, 2009). A color clustering method based on ant colony optimization for the detection of flower boundaries has been notified (Aydın and Ugur, 2011). The search abilities of PSO and ABC have been exploited in multi-level thresholding (Akay, 2013). A multilevel thresholding based on harmony search optimization (HSO) has been presented (Oliva et al., 2013). A gray-level histogram based multilevel thresholding of digital images using bat optimization (BO) has been explained (Rajinikanth et al., 2014). A multi-level image thresholding using Otsu technique and firefly based optimization (FFO) has been notified (SriMadhava Raja et al., 2014). A modified PSO based multilevel threshold has been outlined (Yi et al., 2015). Although these methods offer reasonably good results for image segmentation problems, the improper choice of certain parameters, such as attractiveness and random movement factor in FFO, harmony memory considering rate and pitch adjusting rate in HSO, affects the convergence and leads to suboptimal solution.

More recently, a Dragonfly optimization (DFO), a swarm intelligence based stochastic optimization technique inspired from the static and dynamic swarming behaviors of dragonflies, has been suggested for solving combinatorial optimization problems in (Mirjalili, 2015). Since its introduction, it has been applied to several real world optimization problems (Hamdy et al., 2016; Tiwari et al., 2016) and found to yield satisfactory results. The robustness of the DFO algorithm can be further improved by adaptively adjusting its parameters that have influence on the convergence and the final solution.

The focus of this paper is to develop a self-adaptive scheme for DFO and then use it in developing a robust multilevel segmentation method for processing digital images with a view of obtaining the global best solution and studying its performances on real life and medical images.

2. Dragonfly optimization

The static and dynamic swarming behaviors of dragonflies are the main inspiration of the DFO algorithm, representing the exploration and exploitation phases of meta-heuristic optimization. DFO initially produces a swarm of dragonflies located randomly in the search space. The position of each dragonfly in the solution space represents a potential solution of the optimization problem. Each ith dragonfly is denoted by a vector df_i as (Mirjalili, 2015).

$$df_i = [df_i^1,\ df_i^2,\ \ldots,\ df_i^{nv}] \tag{1}$$

where df_i^j indicates jth position parameter of ith dragonfly and nv represents the number of problem variables.

The search space is limited by the following inequality

$$df^k(min) \leqslant df^k \leqslant df^k(max): \quad k = 1,\ 2, \ldots,\ nv \tag{2}$$

Initially, the positions of the dragonflies are generated from a uniform distribution using the following equation

$$df_i^k = df_i^k(min) + (df_i^k(max) - df_i^k(min)) \times rand \tag{3}$$

Here, $rand$ is a random number in between 0 and 1. A fitness function receives the position of a dragonfly as input and returns a single numerical output value denoting how good the potential solution is. The behavior of swarms are represented through separation, alignment and cohesion with an objective of survival through attraction and distraction, which are mathematically modeled as:

The separation of ith dragonfly, S_i, from its neighbors is computed by

$$S_i = -\sum_{j\in\Psi} df_i - df_j \tag{4}$$

where

Ψ is a set of neighboring individuals

df_i indicates vector of ith dragonfly

The alignment of ith dragonfly, A_i, with its neighbors is calculated by

$$A_i = \frac{\sum_{j\in\Psi} v_j}{nn} \tag{5}$$

where

v_j represents the velocity of jth neighboring dragonfly

nn is the number of neighbors

The cohesion of ith dragonfly, C_i, with its neighbors is evaluated by

$$C_i = \frac{\sum_{j\in\Psi} df_j}{nn} - df_i \tag{6}$$

The attraction of ith dragonfly, F_i, toward a food source is computed by

$$F_i = Food - df_i \tag{7}$$

where *Food* represents the best dragonfly the swarm has seen so far.

The distraction of ith dragonfly, E_i, outward an enemy is computed by

$$E_i = Enemy + df_i \tag{8}$$

where *Enemy* represents the worst dragonfly the swarm has seen so far.

The direction of the movement, $v_i(t+1)$, of ith artificial dragonfly at instant $(t+1)$ from the current position in a search space can be defined by the following velocity vector:

$$v_i(t+1) = (s\,S_i + a\,A_i + c\,C_i + f\,F_i + e\,E_i) + \omega\,v_i(t) \tag{9}$$

where

s, a, c, f and e represent weight factor for separation, alignment, cohesion, food and enemy respectively.

ω indicates inertia weight.

t denotes iteration counter.

The position of ith artificial dragonfly at instant $(t+1)$ can be updated by

$$df_i(t+1) = df_i(t) + v_i(t+1) \tag{10}$$

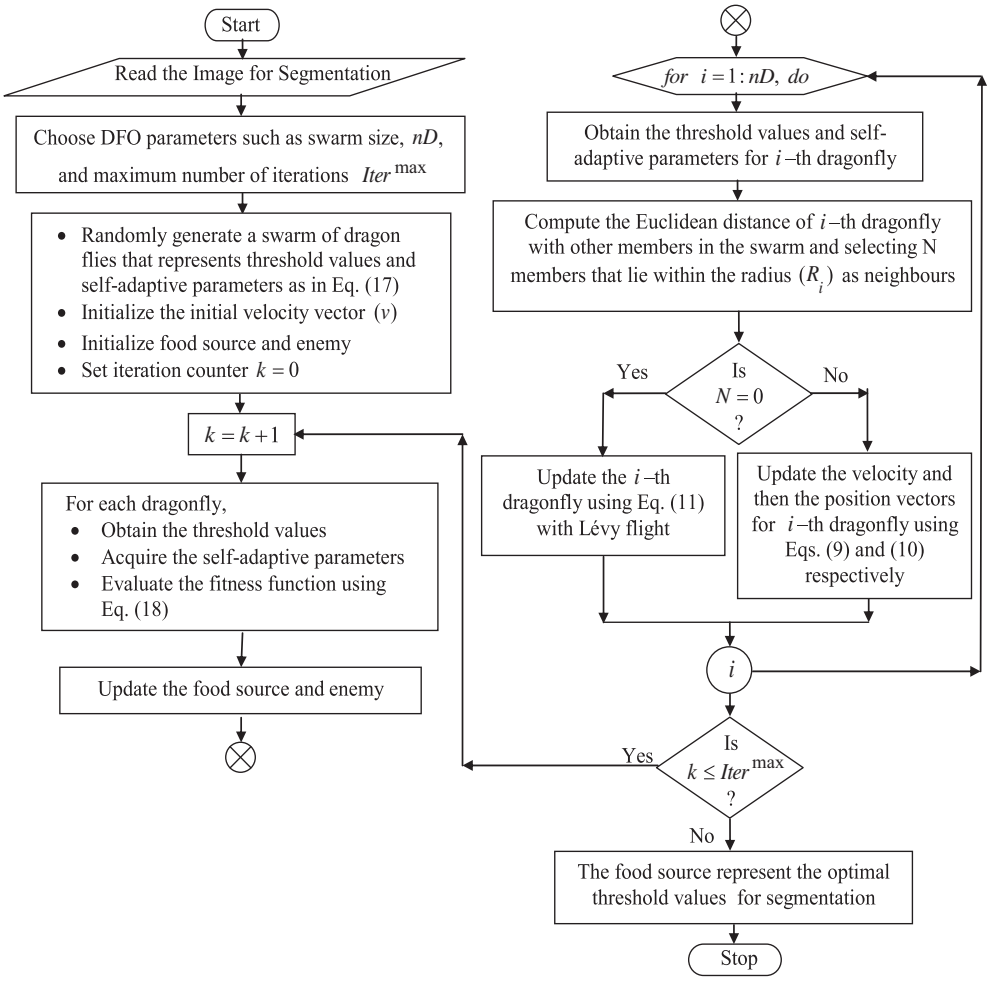

Figure 1 Flow chart of SADFO.

When there is no neighboring solution, the dragonflies are required to fly around the search space using a random walk (Levy's flight) with a view of improving the randomness, stochastic behavior and exploration. In this case, the position of ith artificial dragonfly at instant $(t+1)$ is updated by the following equation:

$$df_i(t+1) = df_i(t) + \Re \times df_i(t) \tag{11}$$

where

$$\Re = 0.01 \times \frac{r_1 \times \sigma}{|r_2|^{1/\beta}} df_i(t) \tag{12}$$

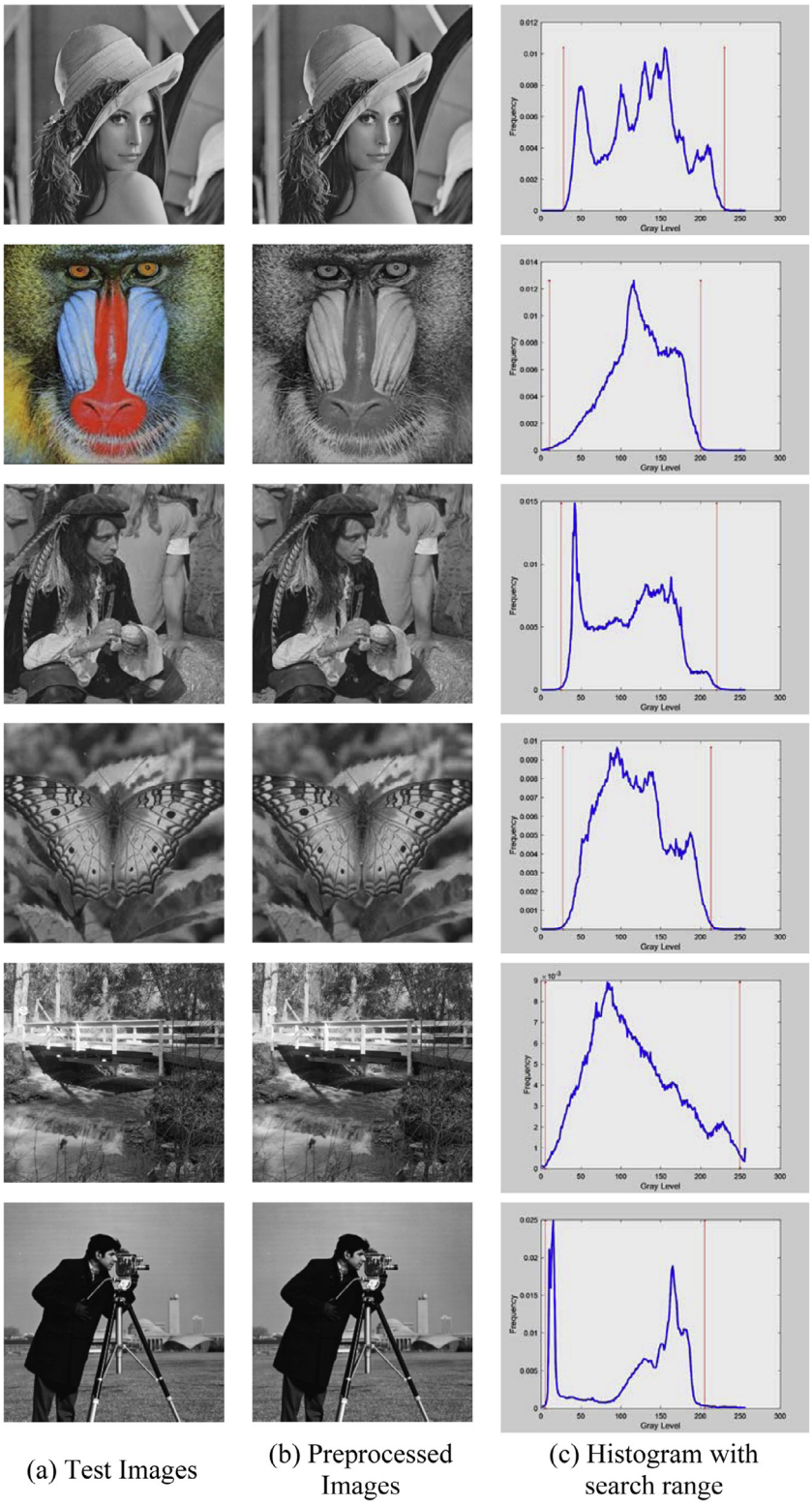

Figure 2 Histogram with search boundaries for first image set.

$$\sigma = \left(\frac{\Gamma(1+\beta) \times \sin\left(\frac{\pi\beta}{2}\right)}{\Gamma\left(\frac{1+\beta}{2}\right) \times \beta \times 2^{(\beta-1/2)}} \right)^{1/\beta} \tag{13}$$

$$\Gamma(x) = (x-1)! \tag{14}$$

r_1 and r_2 are the random numbers in the range of (0, 1)
β is a constant.

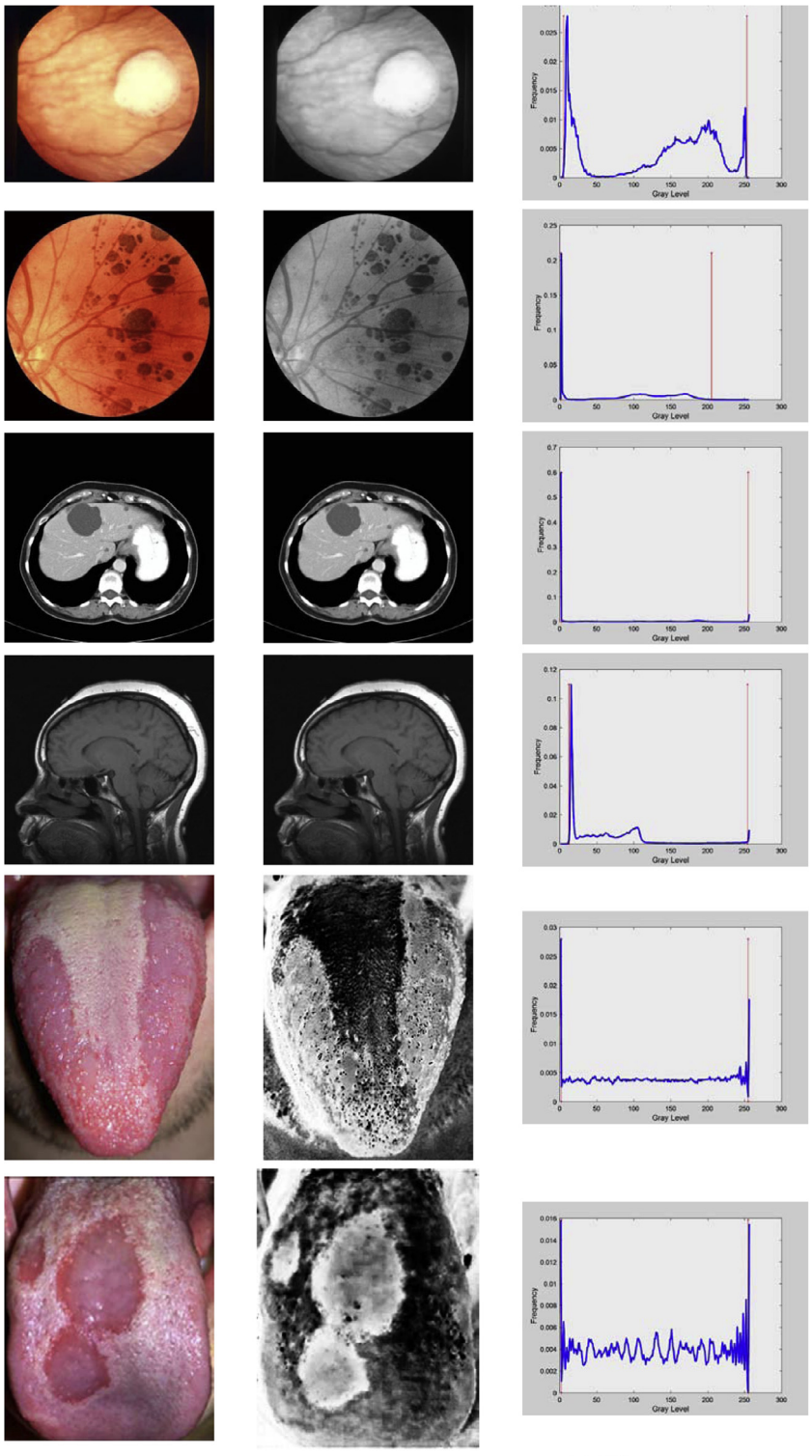

Figure 3 Histogram with search boundaries for second image set.

2.1. Self-adaptive DFO

In the above narrated DFO, different explorative and exploitative behaviors of dragonflies can be achieved by varying separation (s), alignment (a), cohesion (c), food (f), and enemy (e) factors. The dragonflies attempt to align their flying while maintaining appropriate separation and cohesion in a dynamic swarm. In a static swarm, however, alignments are very low while cohesion is high to attack preys. Therefore, high alignment and low cohesion weights are assigned to dragonflies when exploring the problem space; and low alignment and high cohesion when exploiting the problem space. Besides the neighborhood of each dragonfly is chosen by comparing its Euclidean distance with all the dragonflies in the swarm with an assumed radius (R), which is increased proportional to the number of iterations for transition between exploration and exploitation.

The inertia weight (ω) also influences the impact of the prior velocities on the current velocities; and hence controls the trade-off between the global and local exploration abilities. At initial stages of the search, large ω to enhance global exploration is recommended while for last stages, the ω is decreased for better local exploration.

In fact, the selection of these parameters affects the convergence and the final solution of the algorithm. In this paper, the parameters s, a, c, f, e, R and ω are tuned through a self-adaptive mechanism, which effectively leads the algorithm to land at the global best solution with minimum computational effort. Each dragonfly for a given problem with, nv decision variables will be defined to encompass these seven parameters in self-adaptive method as

$$df_i = \left[df_i^1,\ df_i^2,\ \cdots,\ df_i^{nv},\ s_i,\ a_i,\ c_i,\ f_i,\ e_i,\ \gamma_i,\ \omega_i\right] \tag{15}$$

where γ_i denotes radius adjustment factor that controls the radius (R) by the following equation

$$R_i^k = \left(df_i^k(max) - df_i^k(min)\right) \times \gamma_i \tag{16}$$

The typical lower and upper bounds of the parameters s, a, c, f, e, γ, ω are [0, 0, 0, 0, 0, 0, 0] and [0.15, 0.15, 0.15, 2, 0.15, 1, 1] respectively.

Each dragonfly possessing the additional parameters undergoes the whole search process. The DFO offers better offsprings during the search with lower computational effort.

3. Proposed method

Among the available multilevel image thresholding methods, Kapur's entropy (Kapur et al., 1985) based thresholding method has been found to be the most efficient and eminent method for segmentation (Sezgin and Sankur, 2004). The proposed method (SADFO) thus uses Kapur's entropy, which is based on probability distribution of the image histogram and represents the compactness and separability among the classes, and attempts to search the best possible threshold values. The SADFO involves image preprocessing, representation of decision variables and formation of a fitness function.

3.1. Preprocessing

Digital images get corrupted with noise during acquisition, transmission, storage and retrieval processes. The degradation may be in the form of sensor noise, blur due to camera misfo-

Table 1 Optimal threshold levels for first image set.

	Threshold levels	PM	HSO	BO	FFO
Lena	2	98,165	96,163	–	90,148
	3	26,97,165	23,96,163	–	63,119,171
	4	26,83,127,176	23,80,125,173	–	55,100,133,183
	5	26,65,98,139,179	23,71,109,144,180	–	49,98,124,150,185
Baboon	2	98,213	79,143	48,114	90,147
	3	73,135,213	79,143,231	84,95,122	101,148,193
	4	43,91,143,213	44,98,152,231	43,169,193,198	70,104,133,182
	5	35,72,109,152,214	33,74,114,159,231	94,126,128,140,172	71,111,134,167,187
Hunter	2	107,179	92,179	–	–
	3	81,129,181	59,117,179	–	–
	4	70,108,144,182	44,89,133,179	–	–
	5	69,107,145,181,240	44,89,133,179,222	–	–
Butterfly	2	125,226	27,213	–	–
	3	92,150,226	27,120,213	–	–
	4	76,119,164,227	27,96,144,213	–	–
	5	69,105,142,176,227	27,83,118,152,213	–	–
Bridge	2	99,176	99,151	38,146	–
	3	66,130,193	82,119,160	44,120,195	–
	4	55,103,151,200	71,102,130,163	36,81,144,211	–
	5	48,89,130,171,209	62,77,109,137,167	38,85,131,176,212	–
Cameraman	2	127,194	128,196	–	70,148
	3	45,102,195	44, 103, 196	–	51, 119, 163
	4	44,98,146,198	44, 96, 146, 196	–	49, 117, 144, 182
	5	25,61,100,146,198	24, 60,98,146, 196	–	38, 91,137,170,201

cus, relative object camera motion, random atmospheric turbulence, and so on. Image denoising is an important preprocessing task before segmentation. The purpose of denoising is to remove the noise while retaining the edges and other detailed features as much as possible. The linear, median, Winner and recursive filters are used in numerous applications and have proven to be useful for specific tasks (Jun et al. 2016, 2013a, 2013b). In the proposed SADFO, median filter is used for noise removal.

If the digital image is in RGB color space, it is to be converted into two dimensional space, by either converting into gray scale, or transforming it into HSV (or Lab) color space and considering only a two dimensional image component, depending on the type of image and application requirements.

3.2. Representation of a dragonfly

In multi-level thresholding, the original image is divided into nc number of classes by $nc-1$ number of thresholds of $\{T_1, T_2, \ldots, T_{nc-1}\}$. These thresholds act as separators between the consecutive classes of $\{C_1, C_2, \ldots, C_{nc}\}$ in the range of threshold values of $\{[0, \ldots, T_1], [T_1+1, \ldots, T_2], \ldots\ldots, [T_{nc-1}+1, \ldots, L]\}$, where L is the maximum pixel intensity value of the gray scale image. In the SADFO, each dragonfly df_i is defined to denote the threshold levels and the self-adaptive parameters as decision variables in vector form as

$$df_i = [\, T_i^1,\ T_i^2,\ \ldots,\ T_i^{nc-1},\ s_i,\ a_i,\ c_i,\ f_i,\ e_i\ ,\ \gamma_i,\ \omega_i] \tag{17}$$

3.3. Fitness function

The SADFO searches for optimal threshold values by maximizing a fitness function F, in terms of threshold values. The objective function of Kapur's entropy method, an nc dimensional function of maximizing the overall entropy, is considered as the fitness function.

$$\text{Maximize } F = \sum_{k=1}^{nc} H_k \tag{18}$$

where H_k represents kth entropy and is evaluated by

$$\begin{aligned}
H_1 &= \sum_{i=0}^{T_1} \frac{p_i}{\chi_1} \ln\left(\frac{p_i}{\chi_1}\right); & \chi_1 &= \sum_{i=0}^{T_1} p_i \\
H_2 &= \sum_{i=1+T_1}^{T_2} \frac{p_i}{\chi_2} \ln\left(\frac{p_i}{\chi_2}\right); & \chi_2 &= \sum_{i=1+T_1}^{T_2} p_i \\
&\vdots & &\vdots \\
&\vdots & &\vdots \\
H_{nc} &= \sum_{i=1+T_{nc-1}}^{L} \frac{p_i}{\chi_{nc}} \ln\left(\frac{p_i}{\chi_{nc}}\right); & \chi_{nc} &= \sum_{i=1+T_{nc-1}}^{L} p_i
\end{aligned} \tag{19}$$

p_i represents probability distribution at ith intensity level of an image and is calculated by

$$p_i = \frac{h_i}{np}; \quad i \in \{0, 1, \ldots, L\} \tag{20}$$

Table 2 Optimal Threshold Levels for Second Image Set.

	Threshold levels	PM	HSO	FFO
Eye-1	2	35,131	36,130	34,131
	3	35,102,172	36,103,172	36,98,169
	4	35,87,133,186	33,88,131,183	36,82,130,192
	5	34,84,128,167,209	37,81,128,170,208	35,88,131,174,218
Eye-2	2	133,200	132,200	134,201
	3	117,154,200	120,158,200	117,153,200
	4	95,126,160,198	116,155,201,202	106,142,178,204
	5	13,56,90,131,200	11,38,85,138,201	13,73,113,152,199
Liver	2	49,137	50,137	47,135
	3	47,128,202	50,128,201	49,127,204
	4	46,98,153,202	8,69,138,202	8,74,138,202
	5	7,55,99,149,203	6,47,101,155,203	8,52,100,155,202
Head	2	114,187	114,184	113,191
	3	65,113,186	114,159,205	68,115,187
	4	67,114,153,200	66,113,157,206	66,114,158,206
	5	63,118,158,186,222	67,113,148,188,222	67,115,148,186,222
Tongue-1	2	72,156	75,153	80,150
	3	37,142,200	33,147,197	28,151,205
	4	87,104,179,219	91,102,181,220	92,105,177,227
	5	42,72,87,114,183	44,69,97,111,187	44,73,96,110,188
Tongue-2	2	68,176	76,175	75,175
	3	72,122,180	80,126,179	74,119,179
	4	22,123,149,193	17,115,148,190	17,120,152,190
	5	40,53,104,134,192	38,59,101,130,198	36,48,107,143,189

h_i indicates number of pixels that corresponds to ith intensity level
np is the total number of pixels in the image.
χ_i denotes the probability of set C_i.

3.4. Solution method

An initial swarm of dragonflies is obtained by generating random values within their respective limits. The fitness function F

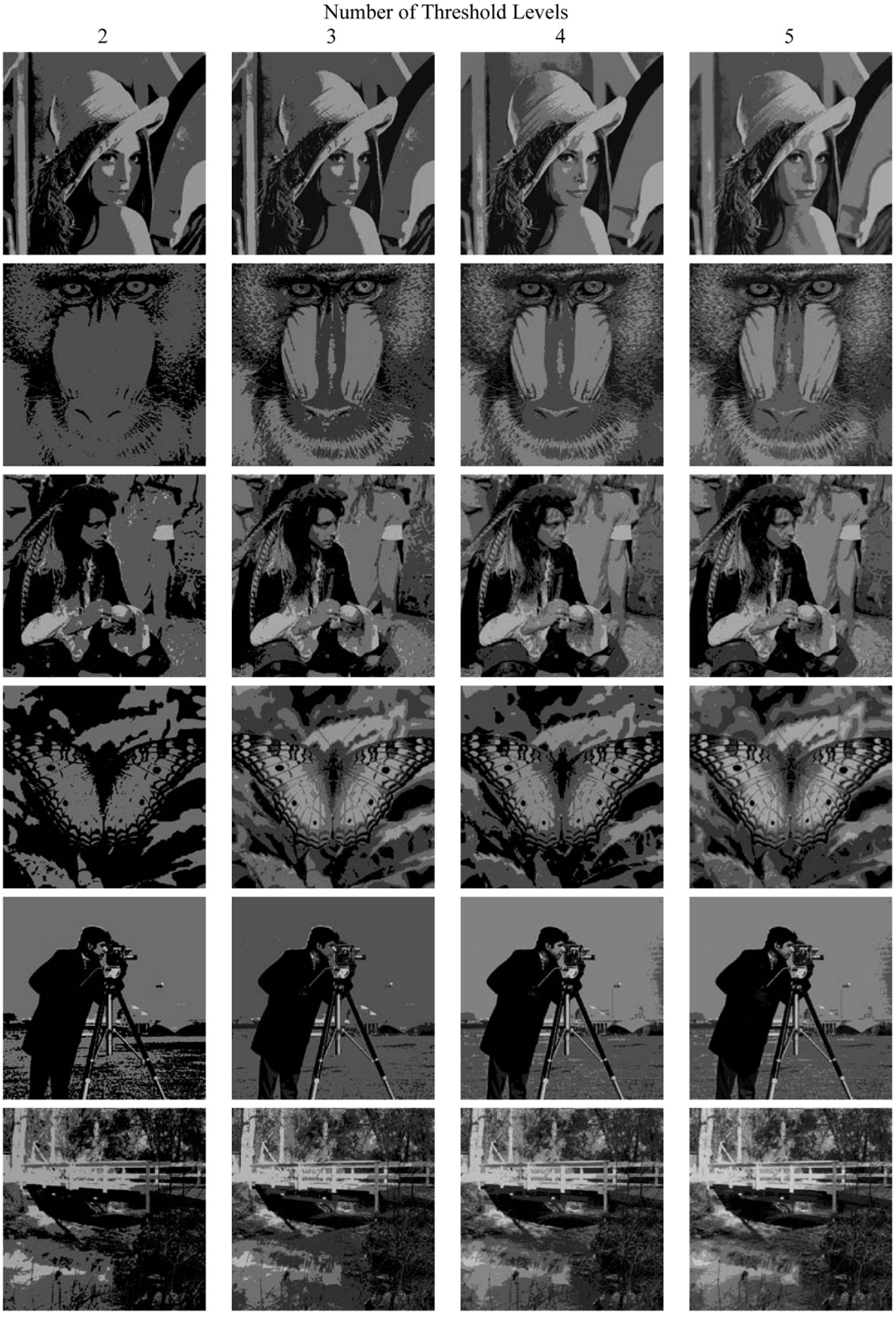

Figure 4 Segmented results for first image set by SADFO.

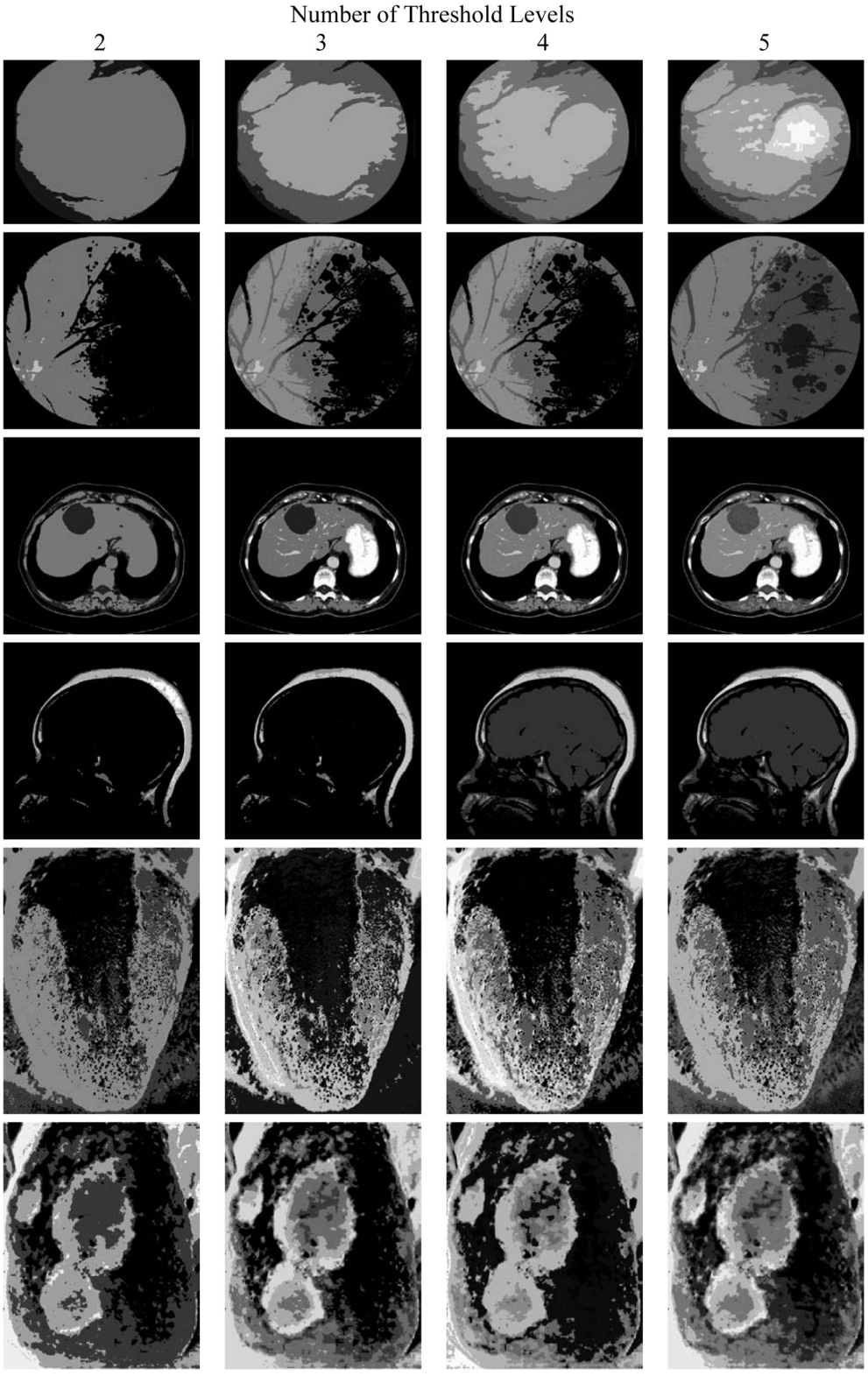

Figure 5 Segmented results for second image set by SADFO.

is calculated by considering the threshold values of each dragonfly; and the exploration and exploitation phases, which represent social interaction of dragonflies in navigating and searching for foods and avoiding enemies, are performed for all the dragonflies in the swarm with a view of maximizing their finesses. The iterative process is continued till convergence. The flow of the SADFO for obtaining the optimal thresholds is shown in Fig. 1.

4. Results and discussions

The proposed SADFO based multilevel segmentation method has been tested on two sets of images. The former one contains six benchmark images of Lena, baboon, hunter, butterfly, bridge and cameraman (Hammouche et al., 2010). These images are converted into (512 × 512 pixels) sized gray scale image with a resolution of 8 bits per pixel. The second set of image comprises six medical images of eyes, liver, head and tongue. As these medical images are rectangular shaped with different sizes, the width of these images is adjusted to have 512 pixels and the height is proportionally altered with a view to have the true shape of the images. Besides, the eye, liver and head images are converted into gray scale, while the tongue images are transformed into HSV color space and their saturation information are considered for further processing. The software packages are developed in Matlab platform and executed in a 2.67 GHz Intel core-i5 personal computer. The results of the SADFO for the first set of images are compared with those of the HSO, BO and FFO based methods (Oliva et al., 2013; Rajinikanth et al., 2014; SriMadhava Raja et al., 2014) with a view of studying and validating the performances. In order to validate the results of SADFO for the second set of medical images, HSO and FFO based methods have also been developed. These methods use the threshold levels as the decision variables and OTSU based between-class variance as the fitness function, as given in the Appendix A (Otsu, 1979). There is no assurance that different executions of these methods converge to the same solution due to the stochastic nature of the SADFO, HSO and FFO, and hence these methods have been run 35 times for each test image and the best ones have been presented.

As the results of the existing methods are available for threshold levels of 2, 3, 4 and 5 for the first set of benchmark images (Oliva et al., 2013; Rajinikanth et al., 2014; SriMadhava Raja et al., 2014), the same number of threshold levels are chosen for testing the SADFO. The original test images, preprocessed images, their histogram and the search boundaries of first and second image sets are given in Figs. 2 and 3 respectively.

The optimal threshold levels obtained by the SADFO are presented along with the existing methods in Tables 1 and 2 respectively for first and second set of images. The resulting segmented images obtained by the SADFO for both image sets are given in Figs. 4 and 5 respectively. The visual analysis of these results clearly indicates that the segmented results are better with more number of threshold levels. In order to quantitatively study the effectiveness of the SADFO, three indices are evaluated for all the segmented results. The first one is the peak signal to noise ratio (PSNR), an index of quality, and used to assess the similarity of the processed (segmented) image against the original image based on the produced mean square error (MSE) (Akay, 2013; Pal et al., 1994). The second one is the structural similarity index (SSI), which is another measure of the image quality through estimating the interdependencies between the original and processed images. It compares the luminance, the contrast and the structure besides satisfying the symmetry and the boundedness. The last one is

Table 3 Comparison of performances metrics for first image set.

		PSNR				SSI				SDI			
		PM	HSO	BO	FFO	PM	HSO	BO	FFO	PM	HSO	BO	FFO
Lena	2	24.6882	14.638	–	23.2027	0.5019	–	–	0.8011	2.14E−14	9.22E−13	–	0.02891
	3	24.7134	16.218	–	20.9014	0.6247	–	–	0.8246	1.99 E−03	2.99E−02	–	0.04903
	4	25.0114	19.287	–	24.1167	0.7014	–	–	0.8165	2.44 E−01	2.77E−01	–	0.31176
	5	25.3331	21.047	–	23.2251	0.7457	–	–	0.8542	2.12 E−01	3.04E−01	–	0.58319
Baboon	2	24.5021	16.016	24.726	23.1159	0.4206	–	0.6672	0.8077	1.58 E−11	6.92E−13	–	0.26681
	3	24.7469	16.016	24.705	21.0002	0.5796	–	0.6762	0.8322	1.96 E−02	1.92E−02	–	0.27916
	4	24.8966	18.485	25.745	24.1883	0.6797	–	0.6860	0.8421	2.84 E−01	5.82E−02	–	0.63441
	5	25.5333	20.507	25.807	21.2683	0.7396	–	0.6896	0.8257	1.29 E−01	4.40E−01	–	0.83551
Hunter	2	24.4475	15.206	–	–	0.3619	–	–	–	6.38E−14	2.30E−12	–	–
	3	24.8195	18.500	–	–	0.4882	–	–	–	5.16 E−05	2.30E−12	–	–
	4	25.1646	21.065	–	–	0.5802	–	–	–	6.16 E−03	1.22E−02	–	–
	5	25.1337	21.086	–	–	0.5778	–	–	–	9.66 E−01	1.84E−12	–	–
Butterfly	2	24.4599	8.1930	–	–	0.2433	–	–	–	2.01 E−09	7.30E−02	–	–
	3	24.7930	13.415	–	–	0.4607	–	–	–	2.91 E−03	6.17E−01	–	–
	4	25.1056	16.725	–	–	0.5847	–	–	–	2.67 E−01	3.07E 00	–	–
	5	25.4528	19.413	–	–	0.6455	–	–	–	2.57 E−00	3.87E 00	–	–
Bridge	2	24.6290	13.529	16.110	–	0.3877	–	0.6274	–	5.22 E−12	4.61E−13	–	–
	3	24.8653	16.806	16.820	–	0.5815	–	0.6530	–	5.78 E−03	7.10E−01	–	–
	4	25.0740	18.902	19.110	–	0.6905	–	0.6556	–	2.82 E−02	2.91E−01	–	–
	5	25.2933	20.268	20.810	–	0.7454	–	0.6638	–	1.62 E−01	3.57E−01	–	–
Cameraman	2	24.7759	13.626	–	25.2568	0.5113	–	–	0.8258	6.04 E−07	2.30E−12	–	0.00176
	3	24.6764	14.460	–	23.2942	0.6053	–	–	0.8432	3.58 E−03	1.55E−02	–	0.11874
	4	25.1169	20.153	–	25.1117	0.6594	–	–	0.8478	4.59 E−02	2.76E−12	–	0.73652
	5	25.2019	20.661	–	26.0004	0.6875	–	–	0.8633	2.93 E−01	5.30E−03	–	0.90362

Table 4 Comparison of performances metrics for second image set.

		PSNR			SSI			SDI		
		PM	HSO	FFO	PM	HSO	FFO	PM	HSO	FFO
Eye-1	2	24.8191	24.7962	24.8123	0.5854	0.5852	0.5831	8.26E−11	4.31E−09	9.44E−06
	3	25.0448	25.0152	25.0268	0.5993	0.5993	0.6002	1.25 E−06	3.99 E−04	4.99E−03
	4	25.3365	25.3107	25.3669	0.6128	0.6179	0.6038	3.38 E−02	4.11 E−03	4.77E−01
	5	25.5135	25.5019	25.4841	0.6058	0.6050	0.5995	1.76 E−00	4.34 E−01	3.01E−00
Eye-2	2	25.7126	25.6775	25.7169	0.4228	0.4225	0.4188	1.29 E−08	6.38E−11	4.30E−07
	3	26.2345	26.2061	26.2218	0.4866	0.4655	0.4883	5.31 E−10	5.36 E−05	4.30E−04
	4	26.8838	26.2545	26.4484	0.6156	0.4845	0.5363	4.18 E−05	6.36 E−02	3.44E−01
	5	26.3175	26.2398	26.5590	0.7290	0.7133	0.7039	4.89 E−03	9.66 E−00	3.81E−01
Liver	2	29.2246	28.7376	29.1625	0.8072	0.8089	0.8022	2.33 E−05	5.44 E−06	1.63E-04
	3	29.2820	29.2255	29.2544	0.8309	0.8249	0.8311	1.33 E−11	5.78 E−05	7.30E−03
	4	29.5461	29.3489	29.3504	0.8649	0.8528	0.8534	4.74 E−03	4.84 E−02	4.93E−03
	5	29.5612	29.5668	29.4994	0.8763	0.8725	0.8715	4.46 E−01	3.64 E−00	3.57E−03
Head	2	24.4610	24.4842	24.4205	0.0742	0.0785	0.0821	4.65E−04	6.01 E−07	4.30E−02
	3	24.7120	24.4466	24.7240	0.3225	0.0858	0.3176	2.00 E−05	3.58 E−03	3.55E−04
	4	24.7712	24.7397	24.6836	0.3275	0.3250	0.3311	5.48 E−01	1.59 E−01	4.76E−01
	5	24.7858	24.7265	24.7014	0.3404	0.3365	0.3330	5.59 E−01	4.93 E−00	5.30E−00
Tongue-1	2	24.7884	24.7632	24.7761	0.5033	0.4883	0.4815	9.24 E−13	3.58 E−11	6.94E−07
	3	25.2390	25.0934	25.1305	0.5582	0.5332	0.5078	6.89 E−08	3.96 E−04	3.94E−04
	4	25.4739	25.4117	25.3529	0.5502	0.5250	0.5247	5.59 E−03	4.81 E−02	5.84E−01
	5	25.6758	25.5950	25.5015	0.6863	0.6681	0.6766	5.23 E−01	3.49 E−01	1.10E−01
Tongue-2	2	24.9877	24.9703	24.9744	0.3936	0.3913	0.3925	2.44E−08	4.03 E−03	7.30E−04
	3	25.2226	25.2196	25.1996	0.5287	0.5084	0.5204	1.29 E−06	4.93 E−03	6.37E−03
	4	25.3865	25.3349	25.2858	0.5123	0.5100	0.5042	1.07 E−03	4.67 E−01	3.07E 00
	5	25.7003	25.4197	25.5531	0.5844	0.5217	0.5521	2.66 E−00	4.57 E−00	3.87E 00

the standard deviation index (SDI), which indicates the amount of dispersion of the data, and evaluated for the results of 35 runs for all the test images with a view to study the stability and consistency of the SADFO. The smaller value of SDI indicates much better stability and consistency and vice-versa. They are mathematically represented as:

$$PSNR = 10\log_{10}\left(\frac{255^2}{MSE}\right) \tag{21}$$

$$SSI(x,y) = \frac{\left(2\mu_x\mu_y + \lambda_1\right)\left(2\sigma_{xy} + \lambda_2\right)}{\left(\mu_x^2 + \mu_y^2 - \lambda_1\right)\left(\sigma_x^2 + \sigma_y^2 - \lambda_2\right)} \tag{22}$$

$$SDI = \sqrt{\sum_{k=1}^{nt} \frac{\left(F_i^{best} - F^{ave}\right)}{nt}} \tag{23}$$

where

F_i^{best} and F^{ave} are the best and average fitness of nt trial solutions respectively

nt represents number of trial solutions

MSE indicates mean squared error and is evaluated by

$$MSE = \sum_{i=1}^{m}\sum_{j=1}^{n}\left(I_{i,j}^{ori} - I_{i,j}^{seg}\right) \tag{24}$$

$I_{i,j}^{ori}$ and $I_{i,j}^{seg}$ are the gray level corresponding to ith row and jth column pixel of original and segmented images respectively

m and n represent the number of rows and columns in image matrix respectively

μ_x and μ_y represent average of x and y respectively

σ_x^2 and σ_y^2 indicate variance of x and y respectively σ_{xy} indicates the covariance of x and y

λ_1 and λ_2 are constants, included to stabilize the division with weak denominator.

The performance metrics of PSNR, SSI, SDI are evaluated for the results of SADFO and compared with those of the existing methods in Tables 3 and 4 respectively for first and second image sets. It is very clear from the results that the PSNR values are comparatively smaller for smaller number of threshold values and increase with the number of threshold levels. The SSI values are also found to increase with the number of threshold values. Besides the PSNR and SSI values are better than the existing approaches, thereby indicating the superior performance of the segmentation process of the SADFO. The smaller values of the SDI indicate that the SADFO offers better stability and consistency. The results clearly exhibit that the SADFO outperforms the existing methods and is suitable for multi-level segmentation of both real life and medical images.

5. Conclusion

DFO is a population based optimization algorithm that simulates the static and dynamic swarming behaviors of dragonflies. The swarming behaviors represent the exploration and exploitation phases of the DFO. A self-adaptive scheme for tuning the DFO parameters has been explained and a methodology involving SADFO for performing multilevel segmentation of digital images has been suggested. The multilevel

segmentation problem has been formulated as an optimization problem and solved using the developed SADFO. The method has been applied on real life and medical images with a view of illustrating the performances. It has been found from the results that the SADFO effectively optimizes the threshold values through exploring the solution space in obtaining the global best solution.

Funding

This research did not receive any specific grant from funding agencies in the public, commercial, or not-for-profit sectors.

Acknowledgements

The authors gratefully acknowledge the authorities of Annamalai University for the facilities offered to carry out this work.

Appendix A.

The decision variables of threshold levels are represented by harmony in HSO and firefly in FFO as

$$harmony_i = [\, T_i^1,\ T_i^2,\ \ldots,\ T_i^{nc-1}] \tag{A.1}$$

$$firefly_i = [\, T_i^1,\ T_i^2,\ \ldots,\ T_i^{nc-1}] \tag{A.2}$$

The fitness function for both the HSO and FFO is built from OTSU based between-class variance as (Otsu, 1979):

$$\text{Maximize } F = \sum_{k=1}^{nc} \chi_k [\, \mu_k - \mu_G]^2 \tag{A.3}$$

where μ_k and μ_G indicate the mean intensity of the set C_k and the global mean intensity of the whole image respectively, and can be calculated by the following equations.

$$\mu_1 = \sum_{i=1}^{T_1} \frac{i \cdot p_i}{\chi_1} \quad \mu_2 = \sum_{i=T_1+1}^{T_2} \frac{i \cdot p_i}{\chi_2} \quad :::::::: \quad \mu_{nc} = \sum_{i=T_{nc-1}+1}^{L} \frac{i \cdot p_i}{\chi_{nc}} \tag{A.4}$$

$$\mu_G = \sum_{i=1}^{L} i \cdot p_i \tag{A.5}$$

References

Akay, B., 2013. A study on particle swarm optimization and artificial bee colony algorithms for multilevel thresholding. Appl. Soft Comput. 13 (1), 3066–3091.

Aydın, D., Ugur, A., 2011. Extraction of flower regions in color images using ant colony optimization. Proc. Comput. Sci. 3 (1), 530–536.

Baradez, M.O., McGuckinb, C.P., Forrazb, N., Pettengell, R., Hoppe, A., 2004. Robust and automated unimodal histogram thresholding and potential applications. Pattern Recogn. 37 (6), 1131–1148.

Li, B.N., Chui, C.K., Chang, S., Ong, S.H., 2011. Integrating spatial fuzzy clustering with level set methods for automated medical image segmentation. Comput. Biol. Med. 41, 1–10.

Bonnet, N., Cutrona, J., Herbin, M., 2002. A no-threshold' histogram based image segmentation method. Pattern Recogn. 35 (10), 2319–2322.

Carvalho, A.T.F., 2007. Fuzzy C-means clustering methods for symbolic interval data. Pattern Recogn. Lett. 28 (4), 423–437.

Chaira, T., 2011. A novel intuitionistic fuzzy C-means clustering algorithm and its application to medical images. Appl. Soft Comput. 11, 1711–1717.

Chen, S.C., Zhang, D.Q., 2004. Robust image segmentation using FCM with spatial constraints based on new kernel-induced distance measure. IEEE Trans. Syst. Man Cybern. Part B Cybern. 34 (4), 1907–1916.

Chuang, K.S., Tzeng, A.L., Chen, S., Wu, J., Chen, T.J., 2006. Fuzzy c-means clustering with spatial information for image segmentation. Comput. Med. Imaging Graph 30, 9–15.

Cinsdikici, M.G., Aydın, D.A., 2009. Detection of blood vessels in ophthalmoscope images using MF/ant (matched filter/ant colony) algorithm. Comput Methods Progr. Biomed. 96 (2), 85–95.

Clausi, D.A., 2002. K-means iterative fisher (KIF) unsupervised clustering algorithm applied to image texture segmentation. Pattern Recogn. 35 (9), 1959–1972.

Comaniciu, D., Meer, P., 2002. Mean shift: a robust approach toward feature space analysis. IEEE Trans. Pattern Anal. Mach. Intell. 24 (5), 1–18.

Dharmendra Tiwari., Nikhil Pachauri., Asha Rani., Vijander Singh., 2016. Fractional order PID (FOPID) controller based temperature control of bioreactor. In: Proceedings of International Conference on Electrical, Electronics, and Optimization Techniques (ICEEOT).

Oliva, D., Erik, C., Gonzalo, P., Daniel, Z., Marco, P.C., 2013. Multilevel thresholding segmentation based on harmony search optimization. J. Appl. Math. http://dx.doi.org/10.1155/2013/575414. Article ID 575414.

Fauvel, M., Tarabalka, Y., Benediktsson, J.A., Chanussot, J., Tilton, J.C., 2013. Advances in spectral-spatial classification of hyperspectral images. Proc. IEEE 101 (3), 652–675.

Hammouche, K., Diaf, M., Siarry, P.A., 2010. Comparative study of various meta-heuristic techniques applied to the multilevel thresholding problem. Eng. Appl. Artif. Intell. 23 (5), 676–688.

Hojjatoleslami, S.A., Kittler, J., 1998. Region growing: a new approach. IEEE Trans. Image Process. 7 (7), 1079–1084.

Jun, Hu., Zidong, W., Steven, L., Huijun, G., 2016. A variance-constrained approach to recursive state estimation for time-varying complex networks with missing measurements. Automatica 64, 155–162.

Jun, Hu, Zidong, W., Bo, S., Huijun, G., 2013a. Quantized recursive filtering for a class of nonlinear systems with multiplicative noises and missing measurements. Int. J. Control 86 (4), 650–663.

Jun, Hu., Zidong, W., Bo, S., Huijun, G., 2013b. Gain-constrained recursive filtering with stochastic nonlinearities and probabilistic sensor delays. IEEE Trans. Signal Process. 61 (5), 1230–1238.

Juang, L.H., Wu, M.N., 2010. MRI brain lesion image detection based on color-converted k-means clustering segmentation. Measurement 43, 941–949.

Kapur, J.N., Sahoo, P.K., Wong, A.K.C., 1985. A new method for gray-level picture thresholding using the entropy of the histogram. Comput. Vision Graphics Image Process. 29, 273–285.

Ma, M., Liang, J., Guo, M., Fan, Y., Yin, Y., 2011. SAR image segmentation based on artificial bee colony algorithm. Appl. Soft Comput. 11 (8), 5205–5214.

Hamdy, M., Nguyen, A.T., Hensen, J.L.M., 2016. A performance comparison of multi-objective optimization algorithms for solving nearly-zero-energy-building design problems. Energy Build. http://dx.doi.org/10.1016/j.enbuild.2016.03.035.

Natarajan, P., Krishnan, N., Kenkre, N.S., Nancy, S., Singh, B.P., 2012. Tumor detection using threshold operation in MR brain images. IEEE Int. Conf. Comput. Intell. Comput., 1–4

Omran, M.G.H., Salman, A., Engelbrecht, A.P., 2005. Dynamic clustering using particle swarm optimization with application in image segmentation. Pattern Anal. Appl. 8 (1), 332–344.

Otsu, N., 1979. A threshold selection method from gray level histograms. IEEE Trans. Syst. Man Cybern. 9 (1), 62–66.

Pal, S.K., Bhandari, D., Kundu, M.K., 1994. Genetic algorithms for optimal image enhancement. Pattern Recogn. Lett. 15 (3), 261–271.

Papamichail, G.P., Papamichail, D.P., 2007. The k-means range algorithm for personalized data clustering in e-Commerce. Eur. J. Oper. Res. 177 (3), 1400–1408.

Rajinikanth, V., Aashitha, J.P., Atchaya, A., 2014. Gray-level histogram based multilevel threshold selection with bat algorithm. Int. J. Comput. App. 93 (16), 1–8.

Sezgin, M., Sankur, B., 2004. Survey over image thresholding techniques and quantitative performance evaluation. J. Electron. Image. 13 (1), 146–168.

Mirjalili, Seyedali, 2015. Dragonfly algorithm: a new meta-heuristic optimization technique for solving single-objective, discrete and multi-objective problems. Neural Comput. Applic.. http://dx.doi.org/10.1007/s00521-015-1920-1.

Shih, F.Y., Cheng, S., 2005. Automatic seeded region growing for color image segmentation. Image Vis. Comput. 23, 877–886.

Skarbek, W., Koschan, A., 1994. A Colour Image Segmentation: A Survey. Technical report. Institute for Technical Informatics, Technical University of Berlin.

SriMadhava Raja, N., Rajinikanth, V., Latha, K., 2014. Otsu based optimal multilevel image thresholding using firefly algorithm. Model. Simul. Eng. http://dx.doi.org/10.1155/2014/794574. Article ID 794574.

Tarabalka, Y., Chanussot, J., Benediktsson, J.A., 2010. Segmentation and classification of hyperspectral images using watershed transformation. Pattern Recogn. 43 (7), 2367–2379.

Xie, K., Yang, J., Zhang, Z.G., Zhu, Y.M., 2005. Semi-automated brain tumor and edema segmentation using MRI. Euro. J. Radiol. 56 (1), 12–19.

Yi, L., Caihong, M., Weidong, K., Jing, L., 2015. Modified particle swarm optimization-based multilevel thresholding for image segmentation. Soft. Comput. 19, 1311–1327.